Research Article

Paleogeographical reconstruction of the western French Alps foreland during the last glacial maximum using cosmogenic exposure dating

Thibault Roattino[1]*, Christian Crouzet[1], Riccardo Vassallo[1], Jean-François Buoncristiani[2], Julien Carcaillet[3], Natacha Gribenski[4] and Pierre G. Valla[3,4]

[1]Univ. Savoie Mont Blanc, Univ. Grenoble Alpes, CNRS, IRD, Univ. Gustave Eiffel, ISTerre. 73000 Chambéry, France; [2]Biogéosciences, UMR 6282 CNRS/Bourgogne Franche-Comté University. 21000 Dijon, France; [3]Univ. Grenoble Alpes, Univ. Savoie Mont Blanc, CNRS, IRD, Univ. Gustave Eiffel, ISTerre. 38000 Grenoble, France. and [4]Bern University, Institute of Geological Sciences. Baltzerstrasse 3, 3012 Bern, Switzerland

Abstract

The extent of glaciers in the western French Alps foreland during the last glacial maximum (LGM, 26.5–19 ka) has not yet been determined, so understanding glacial paleogeography during the LGM remains an open question. This study focuses on the glacial chronology in the western French Alps piedmont using ^{10}Be surface exposure ages on nine glacial boulders and 12 erratic boulders. Results indicate an LGM glacier advance between ca. 24 and 21 ka. During the late LGM, a smaller glacier readvance or stabilization phase occurred at ca. 19 ka, which was followed by a withdrawal phase between ca. 19 and 16.5 ka. Our outcomes show that the LGM extent in the western French Alps was similar or slightly less extensive than the pre-LGM ice extents during the last glacial. Such paleogeography has also been suggested in the western Italian Alps, which share the same accumulation zone with the western French Alps glaciers. The LGM dynamic of the western French Alps foreland glaciers highlighted by our exposure ages is consistent with the timing of the LGM glacier advances and deglaciation with the western Italian ice lobes.

Keywords: LGM, Glacier, Cosmogenic nuclides, western French Alps, Paleogeography

(Received 1 October 2021; accepted 4 May 2022)

INTRODUCTION

For the late Pleistocene (i.e., the last 129 ka), δ^{18}O variations in planktonic fossils from oceanic cores have been used as a proxy for the continental ice volume (Emiliani, 1955; Shackleton, 1987), reflecting global paleoclimatic variations and defining marine isotope stages (MIS). Ice cores from Greenland (Grootes et al., 1993) and Antarctica (Petit et al., 1999) have also provided high-resolution temperature reconstructions mainly from ice isotopic records. From these paleoclimate proxies, it was shown that late Pleistocene temperature minima occur during MIS 4 and mainly during MIS 2 (Bond et al., 1993; Lisiecki and Raymo, 2005). The last glacial maximum (LGM), which occurred during MIS 2, between 26.5–19 ka (Clark et al., 2009) or between 30–16.5 ka (Lambeck et al., 2014), refers to the most recent cold period when the global ice sheet volume reached its maximum.

In the marginal areas of the European Alps, morainic complexes have been recognized and well mapped (Penck and Brückner, 1909; Ehlers et al., 2011, and references therein), indicating the large extent of the Alpine late Pleistocene glaciers that formed broad piedmont lobes. Two main glacier advance phases have been recorded during the LGM in the European Alps. The first one occurred between 24 and 22 ka in the Italian foreland (Monegato et al., 2007; Gianotti et al., 2008, 2015; Ravazzi et al., 2012; Fontana et al., 2014; Scapozza et al., 2014; Ivy-Ochs et al., 2018; Braakhekke et al., 2020; Kamleitner et al., 2022) and in the northern Swiss foreland (Ivy-Ochs et al., 2004; Akçar et al., 2011; Reber et al., 2014; Graf et al., 2015; Ivy-Ochs, 2015), followed by a simultaneous retreat of the northern Swiss foreland lobes from their maximum positions (Ivy-Ochs et al., 2004; Akçar et al., 2011; Reber et al., 2014; Graf et al., 2015; Ivy-Ochs, 2015). The second glacier advance phase happened ca. 21–19 ka on the northern and southern sides of the Alps (Jorda, 1988; Lister, 1988; Monegato et al., 2007; Starnberger et al., 2011; Federici et al., 2012, 2016; Ravazzi et al., 2012; Fontana et al., 2014; Reber et al., 2014; Ivy-Ochs, 2015; Ivy-Ochs et al., 2018; Braakhekke et al., 2020; Kamleitner et al., 2022).

For the western French Alps, until recently, only scarce radiocarbon dates were available (Loebell, 1980; Evin et al., 1985; Mandier, 1988; Mandier and Piegay, 1991; Bossuet et al., 1996; Bintz and Evin, 2002; Mandier et al., 2003; Doyen et al., 2015), and two hypotheses were proposed for the chronology of the Late Pleistocene maximum glacier extent, mainly based on a correlation with isotopic data from Greenland. The first hypothesis proposes a glacial maximum ca. 27 ka and the second hypothesis suggests a glacial maximum ca. 22 ka (Schoeneich, 1998). Studies of the LGM paleogeography of the

western French Alps glaciers were then mainly based only on a morpho-stratigraphical approach (Enay, 1981; Mandier, 1984; Monjuvent, 1988; Kerrien and Monjuvent, 1990), and are not supported by quantitative chronology. More recently, an earlier timing for the glacial maximum has been proposed in the western French foreland (Gribenski et al., 2021). The deposits dated using optically stimulated luminescence (OSL) techniques are well-developed glacio-fluvial sediments that are still preserved today and geomorphologically connected to the morainic landforms associated with the Late Pleistocene maximum glacier advances (Mandier, 1984; Roattino et al., 2021). The results indicate two geometrically similar maximum advances during MIS 4 and late MIS 3, whereas MIS 2 ages were not recorded (Gribenski et al., 2021). Finally, numerical simulations of the last glacial cycle (120–0 ka) in the European Alps indicated the absence of glacier advance on the western French Alps foreland during the LGM (Seguinot et al., 2018), or that the glacier may have spread to a limited extent without reaching the maximum MIS 4/late MIS 3 configurations (Becker et al., 2016; Mey et al., 2016; Višnjević et al., 2020).

The current lack of quantitative data for the LGM period raises the question of glacier paleogeography in the western French Alps foreland during this period. In the western French Alps, ^{10}Be surface-exposure dating spanning the late glacial and the Holocene period has only been applied on the inner valleys (Coutterand and Nicoud, 2005; Cossart et al., 2008, 2012; Perret, 2014; Wirsig et al., 2016; Le Roy et al., 2017; Schwartz et al., 2017; Protin, 2019; Protin et al., 2019; Prud'homme et al., 2020) and not in the foreland area.

In this context, this study aims to address two main questions: Did the glacier reached the foreland during the LGM? And if yes, was the LGM advance similar or significantly less extensive than the earlier advances recorded in the Lyon foreland during the last glacial period? Here we present new ^{10}Be surface exposure dating results that, in concert with geomorphological evidence, we used to define the LGM paleogeography of the western French Alps foreland.

GEOLOGICAL SETTING

Geography and bedrock geology

This study focuses on the western French Alps foreland (east of the city of Lyon, Fig. 1). The highest topographic reliefs in this area belong to the southern Jura (~1100 m asl), Chat Mountain (~1400 m asl), and the subalpine Chartreuse massif (~1800 m asl). The Rhône Valley is a wide valley that separates the southern Jura and Chat Mountain before reaching the foreland. In the southern part of the foreland (Terres Froides, Fig. 1), the highest hills reach ~800 m asl and are comprised of Miocene molasses. The rest of the foreland topography is a low-relief area with an average elevation of 300 m asl, which is formed mainly by Miocene sandstone and conglomerate and by the monoclinal limestone series of the Crémieu plateau (Gigout et al., 1976; David et al., 1978; Monjuvent et al., 1980; Elmi et al., 1986; Kerrien and Monjuvent, 1990).

Glacial geomorphology and paleogeography

The last glacial cycle maximum extent in the study area is characterized by a range of moraine landforms known as the Internal Moraine Complex (IMC) (Buoncristiani and Campy, 2011), delimiting the extent of a wide piedmont lobe, which is called the Lyonnas ice lobe. At the scale of the Lyonnais ice lobe, three main morainic domains can be distinguished. The western morainic domain close to the Dombes plateau, the intermediate morainic domain mainly constituted by the IMC, and the eastern morainic domain located in the Crémieu Plateau and southern Jura (Fig. 1).

A new geomorphological map (Fig 1) of the morainic domains was constructed using high-resolution digital elevation model (DEM) RGE ALTI® with 5 m resolution from French National Institute of Geographic and Forest Information (IGN®), in southern Jura, Terres Froides, Southwestern foreland, Est Lyonnais (Steiner, 2020; Roattino et al., 2021).

According to the provenance of the pebbles, the Lyonnais ice lobe is fed by glaciers flowing from Mont-Blanc, Beaufortain (Mandier et al., 2003; Buoncristiani and Campy, 2011), Tarentaise, and part of the Maurienne accumulation zone (Mandier et al., 2003; Coutterand et al., 2009; Coutterand, 2010) (Fig. 1). Before reaching the piedmont, the ice flowed through the Rhône Valley between the southern Jura and Chat Mountain (Coutterand, 2010).

During its maximum extent, the Lyonnais ice lobe was ~55 km wide and stretched >40 km into the piedmont. It was bounded to the north by the southern part of the Jura Mountains and to the south by the Terres Froides where the ice flowed in narrow valleys (Fig. 1). In southern Jura, the moraine deposits are mainly arcuate with multiple ridges characteristic of ice marginal deposits. In this area, several longitudinal ridges correspond to lateral and frontal moraines (Kerrien and Monjuvent, 1990). In Terres Froides, the morphology of the moraines is constrained by local topography (Fig. 1). Overall, several arcuate moraine ridges can be observed, reflecting several episodes of marginal glacial deposition (Steinfatt, 1975). In the foreland plain, the Lyonnais ice lobe has built well-preserved moraines in the Est Lyonnais area (Fig. 1). These glacial landforms are constituted by several sets of crests highlighting several glacial stages of the Lyonnais ice lobe that have been identified and correlated from morpho-stratigraphic and pedological points of view (Mandier et al., 2003; Steiner, 2020; Roattino et al., 2021).

In the southern Jura, glacial retreat moraines were recognized as frontal and arcuate frontal moraines in valleys behind or topographically below the morainic front attributed to the IMC (Kerrien and Monjuvent, 1990). During the retreat phases of the Lyonnais ice lobe, several series of morainic landforms, generally oriented NE-SW, with single, multiple, long-linear ridges were also deposited on the Crémieu plateau (Fig. 1) (Monjuvent, 1988; Steiner, 2020).

Available chronological data

Available ages, obtained in an attempt to date glacier advances in the study area, come from radiocarbon and OSL techniques. Sampling has focused only on glacio-fluvial and postglacial deposits, and no direct dating of the moraines exists (Loebell, 1980; Vilain et al., 1988; Mandier and Piegay, 1991; Bossuet et al., 1996; Bintz and Evin, 2002; Gribenski et al., 2021) mainly due to the general lack of in-place boulders on moraine crests, especially along the IMC margins in the Lyon foreland.

OSL dating of glacio-fluvial outwash terraces associated with the most external IMC moraines reveal two geometrically similar glacier extents. The earliest of these two glacier extents happened between ca. 70 and 60 ka (MIS 4) and is found locally in the Est Lyonnais area and Southwestern foreland. The youngest of these two glacier advances occurred between ca. 42 and 29 ka (late MIS 3) (Gribenski et al., 2021), consistent with radiocarbon dating collected above the till near the Dombes plateau (Fig. 1) (Evin et al., 1985; Vilain et al., 1988).
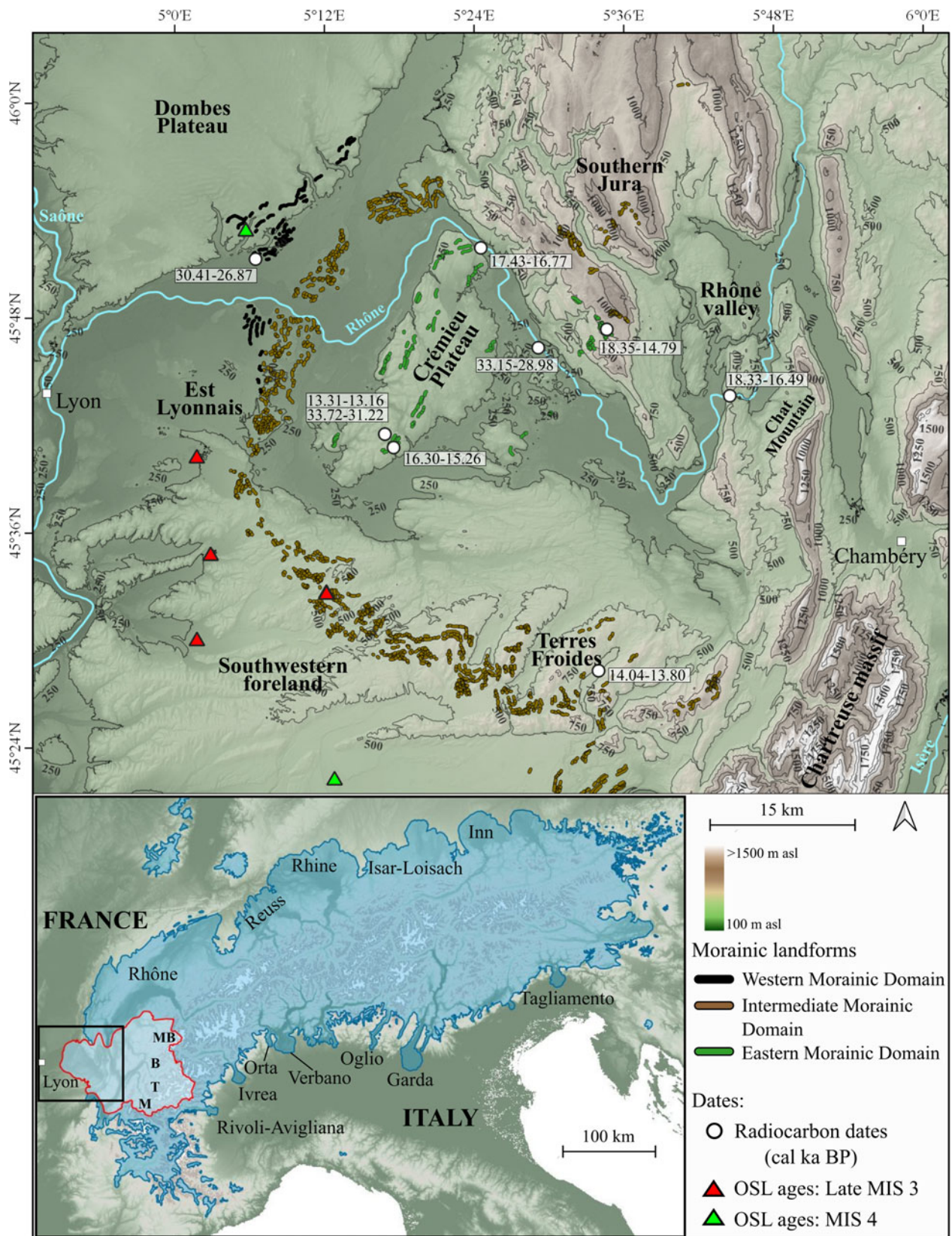
Figure 1. Topographic map showing main relief, rivers, and geomorphological sectors of the study area. Mapping of the western morainic domain (black ridges), intermediate morainic domain (brown ridges), and eastern morainic domain (green ridges) is synthesized from previous work in the area (Steinfatt, 1975; Mandier, 1984; Monjuvent, 1988; Monjuvent and Nicoud, 1988; Kerrien and Monjuvent, 1990; Steiner, 2020; Roattino et al., 2021). Locations of the available radiocarbon ages presented in Table 1 are identified with white dots. Locations of the OSL dating (Gribenski et al., 2021) are marked by the red triangles for the late MIS 3 ages and by the green triangles for the MIS 4 ages. The inset in the lower left corner shows the main European Alpine ice lobes during their maximal extent (updated from Ehlers et al., 2011). The study area is delimited by a black square and the catchment of the Lyonnais ice lobe is demarcated by the red polygon with the main accumulation areas (MB: Mont Blanc; B: Beaufortain, T: Tarentaise, M: Maurienne).

Table 1. Summary of the radiocarbon dates available in the study area. Ages taken from previous studies are given in ka. These data are calibrated into ka Cal BP with the IntCal 20 calibration curve (Reimer et al., 2020) along with the associated uncertainty. For each location, the oldest reliable age is presented.

Location	Sample	Latitude (N)	Longitude (E)	Elevation (m)	Radiocarbon age ^{14}C ka BP	Uncertainty ^{14}C ka BP	cal ka BP	Geological setting	Dated material	Source
Cerin Lake	Ly-5082	45°46.50'	5°33.87'	754	13.68	0.72	18.35–14.79	Lacustrine deposit	Peat	Bossuet et al., 1996
Creys-Malville	Ly-3814	45°45.60'	5°28.36'	142	26.47	0.92	33.15–28.98	Lacustrine deposit	Wood	Mandier, 1988
Garenne Cave	Ly 702 / OxA 8163	45°40.27'	5°16.60'	336	13.15	0.18	16.30–15.26	Cave, human occupation	Reindeer bone	Bintz and Evin, 2002
Moras Lake	Ly-1773	45°41.03'	5°15.93'	283	28.16	0.52	33.72–31.22	Lacustrine deposit	Pollen	Mandier et al., 2003
Moras Lake	SacA-12347	45°41.03'	5°15.93'	250	11.34	0.05	13.31–13.16	Lacustrine deposit	Charcoal	Doyen et al., 2015
Paladru Lake	SacA-20698	45°27.46'	5°32.38'	441	12.02	0.05	14.04–13.80	Lacustrine deposit	Charcoal	Doyen et al., 2015
Porcieu-Amblagnieu	Ly-4814	45°51.27'	5°24.02'	205	14.09	0.12	17.43–16.77	Fluvial deposit	Horse bone	Mandier and Piegay, 1991
Pugnieux	Ly-2318	45°51.17'	5°5.73'	200	24.11	0.90	30.41–26.87	Lacustrine deposit	Peat	Evin et al., 1985
Romains Cave	Ly-16	45°42.56'	5°43.50'	280	14.38	0.38	18.33–16.49	Cave, human occupation	Charcoal	Loebell, 1980

Radiocarbon ages in the study area have been found for the postglacial lacustrine, fluvial, and karst deposits (Table 1). In Est Lyonnais, near the Dombes plateau (Fig. 1), sampled peat deposits above the outer IMC moraine provided a radiocarbon age of 30.41–26.87 cal ka BP (Evin et al., 1985; Vilain et al., 1988). In the Eastern Crémieu plateau, radiocarbon dating was performed at a depth of 66 m within a lacustrine deposit (Mandier, 1988), yielding a radiocarbon age of 33.15–28.98 cal ka BP. Other organic samples (Fig. 1) below lacustrine deposits of Moras Lake provided radiocarbon ages of 33.72–31.22 cal ka BP (Mandier et al., 2003).

A radiocarbon age for human occupation remains yielded an age of 16.30–15.26 cal ka BP (Bintz and Evin, 2002). In the northeastern part of the Crémieu plateau, radiocarbon dating within a fluvial terrace yielded an age of 17.43–16.77 cal ka BP (Mandier and Piegay, 1991). In southern Jura, a lacustrine deposit yielded radiocarbon ages of 18.35–14.79 cal ka BP (Bossuet et al., 1996). Other lacustrine deposits in the Terre Froides and Crémieu areas provided radiocarbon ages of 14.04–13.80 cal ka BP and 13.31–13.16 cal ka BP, respectively (Doyen et al., 2015). Lastly, in the very inner zone (Rhône Valley, Fig. 1), radiocarbon dating suggested the first human settlements at 18.33–16.49 cal ka BP (Table 1).

MATERIALS AND METHODS

Sites and sampling strategy for terrestrial cosmogenic nuclide analyses

Timing of the glaciations was determined by cosmogenic exposure dating on erratic and glacial boulders using terrestrial cosmogenic nuclide ^{10}Be. Nine glacial boulders and 12 erratic boulders were described and sampled with the aim to track the LGM glacial deposits. On this basis, the investigated areas are located on the intermediate and eastern morainic domains, and in more internal regions of the foreland (Fig. 1). However, on the Southwestern foreland and Est Lyonnais sectors, glacial and erratic boulders for ^{10}Be exposure dating are very scarce. Indeed, the dense urbanization and agriculture in this area are probably responsible for the destruction or displacement of boulders, which further reduces opportunities for sampling. Only one large boulder (ART 18-01) is still preserved within the intermediate morainic domain and is located in the Southwestern foreland (Figs. 1, 2). Better preserved glacial morphologies and/or boulders were surveyed in less anthropized areas: the southern Jura, the Terres Froides, and the Rhône Valley (Fig. 3). Nevertheless, large boulders ($>$1 m^3) are sparse, which limited the number of samples per location and required selecting the best boulders. In the field, the biggest, well-anchored, and quartz-rich boulders were chosen preferentially to minimize potential late remobilization, post-abandonment displacement, as well as sustainable burial. The glacial boulders sampled are located on moraine ridges, while erratic boulders are located on bedrock or till deposits (Figs. 2, 3). A hammer, chisel, and angle grinder were used to sample rock chips measuring 4 cm thick. Sampling strategy targeted the top of the boulders to minimize the effect of snow and/or sediment burial through time. Topographic shielding values were measured using a clinometer and a compass.

Analytical procedure

Rock samples were prepared at the GTC platform (ISTerre, Grenoble, France). Samples were crushed and sieved to keep the

Figure 2. Examples of sampled boulders on the southern Jura: INN 18-04 (**A**); Rhône Valley: CUL 20-01 (**B**) and CRV 20-01 (**C**); Crémieu plateau: TRE 18-01 (**D**); Southwestern foreland: ART 18-01 (**E**); and Terres Froides: MIR 20-02 (**F**).

grain size between 200 and 500 μm. The magnetic fraction was isolated using a Frantz© magnetic separator, then quartz was isolated from the other minerals by selective dissolution with several etchings by a mixture H_2SiF_6 (2/3) and HCl (1/3). Quartz grains were etched three times with concentrated hydrofluoric acid (HF) in order to remove the atmospheric ^{10}Be fraction. Approximately 0.5 g of the Be standard solution was used to spike the quartz samples (see Table 3 for details).

The ^{10}Be target was prepared following the protocol of Brown et al. (1991), modified by Merchel and Herpers (1999). After total dissolution by concentrated HF, ^{10}Be was extracted using chromatography techniques using anionic and cationic exchange resins (Dowex 1X8 and Dowex 50WX8). Before conditioning for the AMS analysis, the Be target was oxidized to beryllium oxide (BeO) by heating to 900°C. The beryllium ratio ($^{10}Be/^{9}Be$) was measured using accelerator mass spectrometry at the ASTER AMS facility (Aix en Provence, France) (Arnold et al., 2010). The $^{10}Be/^{9}Be$ ratio was normalized with in-house CEREGE standard reference material (called STD-11; Braucher et al., 2015) with a theoretical ratio of $1.191/10^{11}$.

Age calculation

The online calculator Cosmic Ray Exposure Program (CREP) (Martin et al., 2017) was used to calculate the surface ^{10}Be

exposure ages. The production rate scaling scheme used is the LSD model (Lifton et al., 2014), with the ERA-40 database (Uppala et al., 2005), used to calculate an atmospheric pressure and the VDM geomagnetic record described by Lifton (2016). Scaled production rate based on the Chironico landslide production rate calibration was used (Claude et al., 2014). These parameters were corrected for sample thickness (4 cm) and sample density ($2.65\ g/cm^3$), and were scaled with the sample elevation, latitude, longitude, and topographic shielding correction (Table 2). Surface-exposure ages were calculated with the null erosion rate; therefore, the ages are the minimum estimates. No correction for snow effect was applied since no information about the snow cover record over time is available for the studied area. The present-day snow-covered period at the study area is short (1–2 weeks) and insignificant (<20 cm). Therefore, the snow effect on the surface-exposure ages can be considered as negligible.

RESULTS

Exposures ages are grouped into fives sectors: Southern Jura, Terres Froides, Southwestern foreland, Crémieu plateau, and Rhône Valley (Fig. 4). We obtained 21 terrestrial cosmogenic nuclides dates, 20 of them distributed between 23.8 ± 1.1 ka and 2.9 ± 0.2 ka, with one much older sample at 496.9 ± 19.2 ka (Table 3).
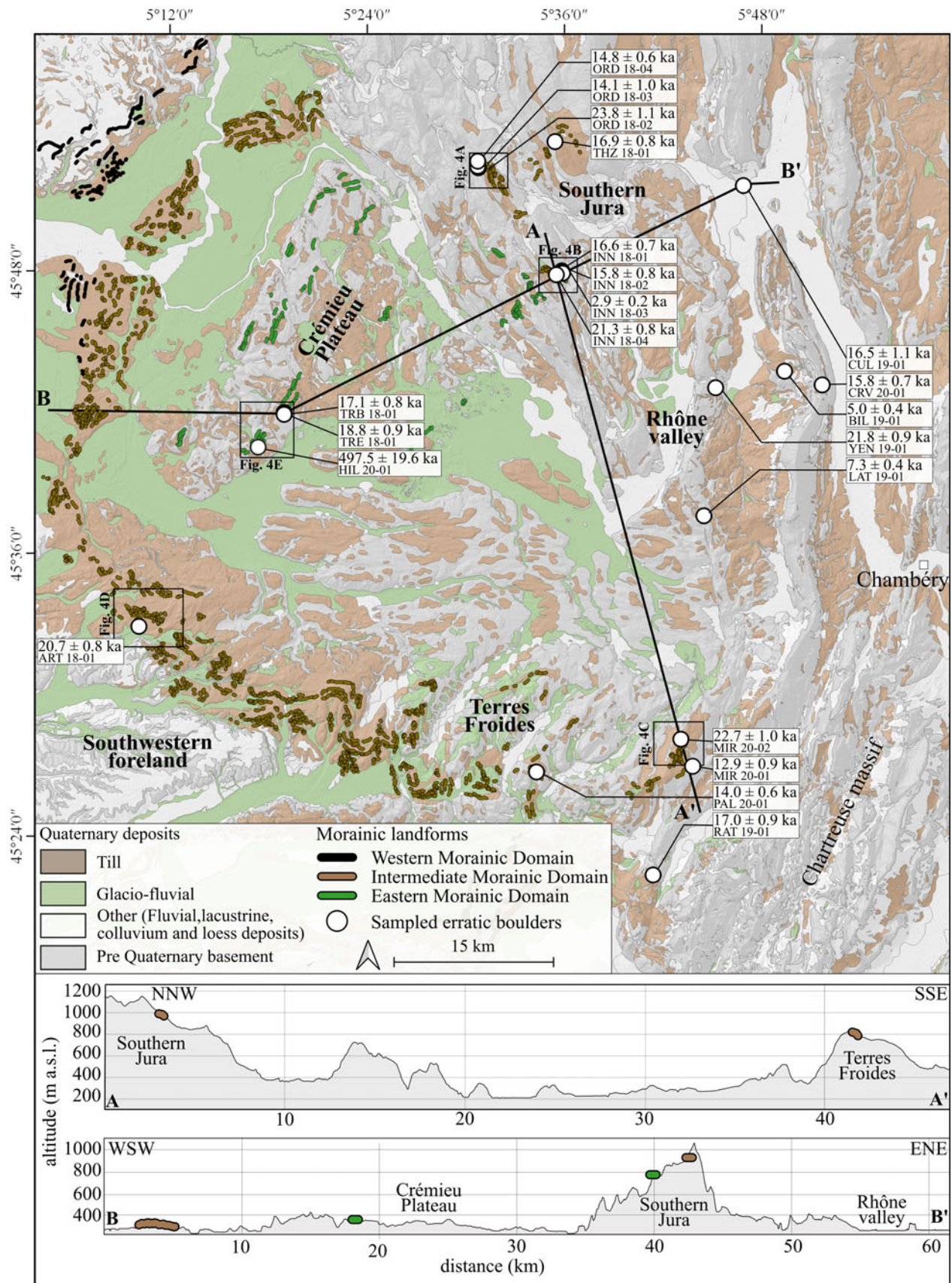
Figure 3. Simplified geological map with Quaternary units from the French Geological Survey (BRGM) (Gigout et al., 1976; David et al., 1978; Monjuvent et al., 1980; Elmi et al., 1986; Kerrien and Monjuvent, 1990) and location of the western morainic domain (black), intermediate morainic domain (brown), and eastern morainic domain (green), annotated with sampling locations (white circles, with their respective labels and ^{10}Be surface-exposure ages). Locations of figure 4A–E indicated by black squares. Topographical cross-sections A-A' and B-B' show the main sampling sectors and locations of the moraines.

Table 2. Geographic coordinates, site information, and apparent size of sampled boulders.

Sample	Areas	Latitude	Longitude	Elevation	Sampling year	Lithology	Geomorphological position	Sample information
		N	E	m asl				Apparent size (length*width*height, m)
HIL 20-01	Crémieu plateau	45°40.25′	5°16.63′	346	2020	Polygenic conglomerate	Boulder on morainic crest	4.2*1.1*2.7*
TRB 18-01		45°41.69′	5°18.27′	339	2018	Polygenic conglomerate	Boulder on morainic crest	9.0*3.7*3.5
TRE 18-01		45°41.61′	5°18.26′	340	2018	Polygenic conglomerate	Boulder on morainic crest	6.5*4.0*3.0
BIL 19-01	Rhône Valley	45°42.76′	5°48.65′	410	2019	Micaschist	Boulder on till	2.5*1.5*0.5
CRV 20-01		45°42.11′	5°50.90′	824	2020	Granite	Boulder on till	2.5*1.2*0.7
CUL 19-01		45°50.71′	5°46.55′	300	2019	Schist	Boulder on the bedrock	4.0*2.0*2.0
LAT 19-01		45°36.73′	5°43.46′	856	2019	Granite	Boulder on till	1.5*0.8*0.7
YEN 19-01		45°42.16′	5°44.44′	350	2019	Schist	Boulder on the bedrock	2.0*1.0*0.5
INN 18-01	Southern Jura	45°47.34′	5°35.36′	1113	2018	Schist	Boulder on till	1.0*0.6*0.4
INN 18-02		45°47.29′	5°35.38′	1099	2018	Schist	Boulder on till	1.2*0.9*0.8
INN 18-03		45°47.24′	5°35.40′	1087	2018	Schist	Boulder on till	1.0*0.5*0.5
INN 18-04		45°47.18′	5°35.02′	972	2018	Quartzite	Boulder on morainic crest	5.0*2.4*2.0
ORD 18-02		45°51.83′	5°30.50′	826	2018	Schist	Boulder on morainic crest	1.3*1.2*0.8
ORD 18-03		45°51.90′	5°30.47′	817	2018	Quartzite	Boulder on morainic crest	1.5*1.2*0.9
ORD 18-04		45°52.12′	5°30.47′	807	2018	Schist	Boulder on morainic crest	1.3*1.2*0.5
THZ 18-01		45°52.84′	5°35.21′	864	2018	Flysch	Boulder on morainic crest	1.2*1.0*0.9
ART 18-01	Southwestern foreland	45°32.78′	5°9.12′	439	2018	Micaschist	Boulder on morainic crest	12.0*6.0*3.5
MIR 20-01	Terres Froides	45°26.13′	5°42.27′	696	2020	Micaschist	Boulder on till	2.0*1.7*1.5
MIR 20-02		45°27.30′	5°41.61′	788	2020	Granite	Boulder on till	4.1*3.4*3.1
PAL 20-01		45°26.11′	5°32.84′	795	2020	Amphibolite	Boulder on till	3.0*1.2*1.0
RAT 19-01		45°21.57′	5°39.66′	670	2019	Granite	Boulder on till	1.5*1.3*1.0

Table 3. Cosmogenic-exposure data. The surface-exposure ages are calculated with a zero-erosion rate. The scale scheme used for the in situ cosmogenic nuclide production rates is the LSD scaling scheme given by Lifton et al. (2014). The atmospheric model considered is the ERA40 model (Uppala et al., 2005). The geomagnetic database used is the VDM, provided by Lifton (2016). Production rates are scaled from the reference Chironico production rate (Claude et al., 2014). Thickness is ∼4 cm for all samples. Spike (a) = Scharlau beryllium standard solution, 998 mg/L; (b) = LN2C, 3025 mg/L.

Sample	Areas	Blank $^{10}Be/^{9}Be$	Blank $^{10}Be/^{9}Be$ uncertainty	$^{10}Be/^{9}Be$ (blank corrected)	$^{10}Be/^{9}Be$ uncertainty	Mass dissolved quartz	Mass spike ^{9}Be	Spike concentration	Shielding factor	Scaled production rates Value	Scaled production rates Uncertainty	^{10}Be concentration Value	^{10}Be concentration Uncertainty	Ages with null denudation rate Value	External uncertainty	Internal uncertainty
			%	at/g	%	g	mg	mg/L		atoms/g/yr		x10³ atoms/gQtz		ka		
HIL 20-01	Crémieu plateau	8.32x10-15	9.80	3.567x10-13	3.088	5.21	0.5240	998(a)	1.000	5.4912	0.132	2333.5	74.43	496.91	19.20	15.07
TRB 18-01		2.64x10-15	13.66	4.959x10-14	4.200	17.69	0.1542	3025(b)	1.000	5.3248	0.128	87.39	3.93	17.08	0.84	0.74
TRE 18-01		2.64x10-15	13.66	6.329x10-14	4.313	20.38	0.1538	3025(b)	1.000	5.3248	0.128	96.56	4.38	18.81	0.93	0.82
BIL 19-01	Rhône Valley	8.32x10-15	9.80	1.716x10-14	4.240	37.42	0.5136	998(a)	0.996	5.4496	0.131	26.16	2.07	4.99	0.40	0.38
CRV 20-01		8.32x10-15	9.80	1.399x10-13	3.221	64.19	0.5133	998(a)	0.994	8.1952	0.197	124.99	4.32	15.82	0.65	0.54
CUL 19-01		8.32x10-15	9.80	1.853x10-14	4.330	19.74	0.5112	998(a)	1.000	5.1584	0.124	81.68	5.14	16.50	1.08	1.01
LAT 19-01		8.32x10-15	9.80	1.859x10-14	4.945	25.04	0.5001	998(a)	1.000	8.2784	0.199	58.60	3.43	7.33	0.43	0.39
YEN 19-01		8.32x10-15	9.80	1.260x10-13	3.098	58.66	0.5131	998(a)	0.998	5.4080	0.130	113.44	3.84	21.80	0.85	0.69
INN 18-01	Southern Jura	2.64x10-15	13.66	1.470x10-13	3.400	27.39	0.1546	3025(b)	1.000	10.5248	0.253	167.69	5.84	16.56	0.68	0.56
INN 18-02		2.64x10-15	13.66	1.328x10-13	4.156	26.30	0.1547	3025(b)	1.000	10.4000	0.250	157.91	6.72	15.79	0.75	0.65
INN 18-03		2.64x10-15	13.66	2.224x10-14	5.565	25.19	0.1550	3025(b)	1.000	9.8592	0.237	27.67	1.78	2.91	0.20	0.19
INN 18-04		2.64x10-15	13.66	1.565x10-13	3.092	25.40	0.1546	3025(b)	0.997	9.4016	0.226	192.48	6.10	21.32	0.80	0.64
ORD 18-02		2.64x10-15	13.66	6.604x10-14	4.050	10.73	0.1535	3025(b)	0.999	8.3616	0.201	190.93	8.13	23.81	1.12	0.97
ORD 18-03		2.64x10-15	13.66	1.046x10-13	6.848	29.60	0.1543	3025(b)	0.999	8.1120	0.195	110.21	7.75	14.08	1,00	0.95
ORD 18-04		2.64x10-15	13.66	7.159x10-14	3.623	19.19	0.1529	3025(b)	1.000	8.0704	0.194	115.28	4.38	14.83	0.64	0.54
THZ 18-01		2.64x10-15	13.66	9.243x10-14	3.757	20.97	0.1550	3025(b)	0.999	8.5280	0.205	138.04	5.38	16.86	0.75	0.63
ART 18-01	Southwestern foreland	2.64x10-15	13.66	1.090x10-13	3.200	28.85	0.1525	3025(b)	1.000	5.7810	0.141	116.52	3.85	20.71	0.80	0.65
MIR 20-01	Terres Froides	8.32x10-15	9.80	1.050x10-14	4.369	39.85	0.5067	998(a)	0.998	7.2384	0.174	89.92	5.63	12.94	0.85	0.80
MIR 20-02		8.32x10-15	9.80	1.090x10-14	4.239	22.54	0.5045	998(a)	0.994	8.0288	0.193	174.03	6.49	22.72	0.96	0.81
PAL 20-01		8.32x10-15	9.80	1.403x10-14	4.221	48.48	0.5128	998(a)	1.000	7.9040	0.190	106.66	3.93	14.00	0.59	0.50
RAT 19-01		8.32x10-15	9.80	1.653x10-14	4.950	25.53	0.5140	998(a)	0.993	7.1136	0.171	115.35	5.50	16.96	0.87	0.78
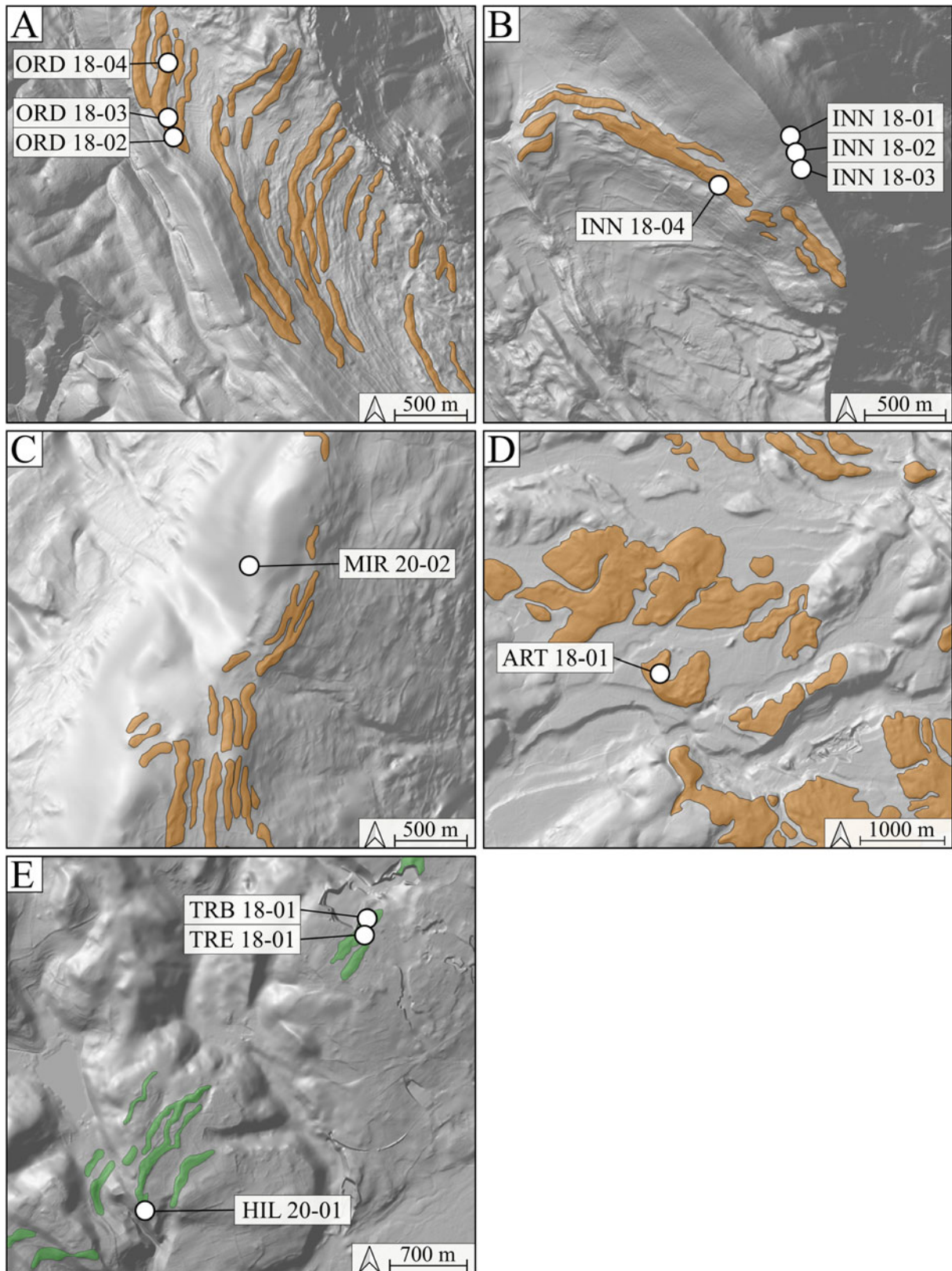
Figure 4. Inset maps (locations given on Fig. 3) from the DEM showing morainic landforms and OSL sampling sites of ORD (**A**) and INN (**B**) boulders in southern Jura, MIR 20-02 (**C**) in Terres Froides, ART 18-01 (**D**) in the Southwestern foreland, and TRB 18-01, TRE 18-01, HIL 20-01 in Crémieu plateau.

Eight boulders were sampled in the southern Jura area, at altitudes between 800–1100 m asl (Table 2) and located on or close to well-preserved arcuate moraines. ORD 18-02, ORD 18-03, and ORD 18-04 glacial boulders are located on a frontal morainic crest (Fig. 4A) and give dates of 23.81 ± 1.12 ka, 14.08 ± 1.01 ka, and 14.83 ± 0.64 ka, respectively (Table 3; Fig. 4). THZ 18-01 glacial boulder lies on a lateral morainic crest (Fig. 3) and provides a date of 16.86 ± 0.75 ka (Table 3; Fig. 3).

INN 18-01, INN 18-02, and INN 18-03 erratic boulders, which are located on a till deposit, provide surface-exposure ages of 16.56 ± 0.68 ka, 15.79 ± 0.75 ka, and 2.91 ± 0.20 ka, respectively. INN 18-04 glacial boulder lies within a well-preserved frontal moraine (Fig. 4B) and yields a date of 21.32 ± 0.80 ka (Table 3; Fig. 3).

Four erratic boulders were sampled in the Terres Froides, between 670–800 m asl. Erratic boulders MIR 20-01, MIR 20-02, PAL 20-01, and RAT 19-01 are located on till. They are not associated with a clear morphologic feature. Nevertheless, the area corresponds to the intermediate morainic domain (Fig. 4). These erratic boulders provide surface exposure ages of 12.94 ± 0.85 ka, 22.72 ± 0.96 ka, 14.00 ± 0.59 ka, and 16.96 ± 0.87 ka, respectively (Table 3; Fig. 4).

ART 18-01 is the only glacial boulder sampled in the Southwestern foreland. It lies farther west, at 440 m asl, on a hummocky moraine (Table 2; Fig. 4D), and yields an age of 20.71 ± 0.80 ka (Table 3; Fig. 4).

Glacial boulders on the Crémieu plateau are located near the southern margin of this topographic high. Three glacial boulders (TRB 18-01, TRE 18-01, and HIL 20-01) were sampled on a linear morainic ridge (Fig. 4E), at an altitude of 340 m asl (Table 2). These three samples yield ages of 17.08 ± 0.84 ka, 18.81 ± 0.93 ka, and 496.91 ± 19.20 ka, respectively (Table 3; Fig. 4).

The last five sampled erratic boulders (CUL 19-01, YEN 19-01, CRV 20-01, BIL 19-01, and LAT 19-01) are not in the foreland and located in a more internal zone to the east, within the Rhône Valley, located between 300–850 m asl (Table 2). Two boulders (CUL 19-01 and YEN 19-01) lie directly on the bedrock. The three other boulders (CRV 20-01, BIL 19-01, and LAT 19-01) are associated with glacial deposits, but without clear landforms (Table 2; Fig. 3). They provide surface-exposure ages of 16.50 ± 1.08 ka, 21.80 ± 0.85 ka, 15.28 ± 0.65 ka, 4.99 ± 0.40 ka, and 7.33 ± 0.43 ka, respectively (Table 3; Fig. 3).

DISCUSSION

Terrestrial cosmogenic nuclides dating

Two types of geological processes may alter interpretation of the exposure ages on erratic and glacial boulders and induce subsequent erroneous chronological conclusions (Brown et al., 2005; Chevalier et al., 2005; Applegate et al., 2007; Barrows et al., 2007). The first process is the prior exposure to the cosmic rays inducing additional cosmogenic nuclides concentration, also called inheritance. This inherited concentration produces an apparent exposure age older than the true deposition age of the target moraine. The other process is the incomplete postdepositional exposure because of shielding due to burial into a moraine or till. The subsequent exhumation yields reduced cosmogenic nuclides concentration with respect to a full exposure at the surface since deposition. This incomplete exposure induces apparent younger exposure age than the true deposition age. Boulders with significant pre-exposure inheritance are not

predominant in glacial contexts because of significant glacier erosion and ice shielding. Incomplete exposure is much more frequent and is the principal source of error in age interpretation (Putkonen and Swanson, 2003; Briner et al., 2005; Heyman et al., 2011, 2016). Considering this assumption, the surface-exposure age can be assessed as a minimum age for the deposition. This assumption is classically used in similar glacier contexts in the Alpine foreland (Ivy-Ochs et al., 2018; Kemleitner et al., 2022). For each site with multiple samples, the oldest exposure age is retained and considered as closest to the real age of the deposit. The preferred age is often derived from the tallest boulder in the most stable position (Putkonen and Swanson, 2003; Heyman et al., 2016; Tomkins et al., 2021). We consider the calculation of mean ages as not reliable in this case. For each site with a single sample, the exposure age is considered as a minimum age unless contradictory with the morpho-stratigraphical position of the boulder at the regional scale.

Southern Jura

According with their geological and geomorphological setting, the three sites (INN, ORD, and THZ) of this area belong to the same glacial stage.

For the multi-sampled INN site (Fig. 3), the retained age of INN 18-04 at 21.32 ± 0.80 ka corresponds to the oldest sample, even if it is not the highest in elevation (∼140 m difference with highest boulder). INN 18-04 is the tallest erratic boulder sampled on the southern Jura (Fig. 2; Table 2), thus limiting incomplete exposure by burial.

For the ORD site (Fig. 3), the three boulders have a similar size, are located on the top of a well-defined morainic crest, and do not exceed 1 m height above the ground (Table 2). The retained age corresponds to the oldest sample ORD 18-02 at 23.81 ± 1.12 ka.

The THZ site (Fig. 3) contains only one boulder. It is located on the internal slope of the moraine and does not protrude much from the ground (∼1 m) (Table 2), making it susceptible to an incomplete exposure by burial or gravitational processes. According to the morphostratigraphical relationship of INN, ORD, and THZ, the age of THZ 18-01 at 16.86 ± 0.75 ka may be considered as underestimated.

For the southern Jura area, the two dated boulder sites (ORD and INN) provide similar oldest exposure ages of 23.81 ± 1.12 ka and 21.32 ± 0.80 ka, respectively, in accordance with the LGM. These dated glacial landforms are the outermost moraines of the southern Jura. No morainic landform attributable to older glacier advances occurs beyond the dated moraines complex, only patches of undated till exist.

Terres Froides

The oldest exposure age of the Terres Froides (Fig. 3) is MIR 20-02 (Fig 2F) at 22.72 ± 0.96 ka, which corresponds to the tallest boulder (Fig. 2; Table 2), limiting incomplete exposure by burial. Similar to the southern Jura area, this age corresponds to the LGM.

MIR 20-02 is not directly located on a morainic landform, but is a few hundred meters from a moraine of the same altitude (Fig. 4C). The age of the closest moraine should be comparable to the exposure age of the boulder. The elevation of this moraine is between 140–50 m below the highest and oldest moraines of the Terres Froides. This geomorphological evidence proves preservation of prior older moraines located topographically above the
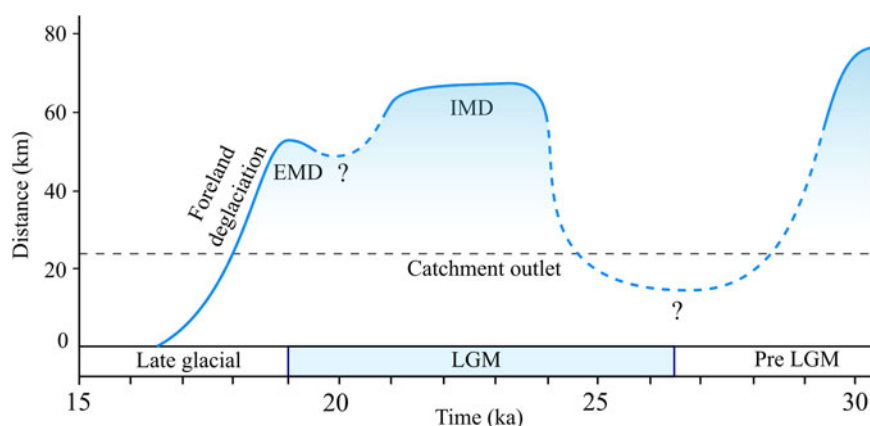
Figure 5. Time- distance diagram for the last glacial cycle glacier advances and retreat of the Lyonnais ice lobe based on OSL, ^{14}C, and our exposure ages. IMD = Intermediate Morainic Domain; EMD = Eastern Morainic Domain. Distance origin is located at the level of CUL 19-01 boulder.

LGM moraines dated by our exposure ages. According to Steinfatt (1975) and Mandier (1984), these higher moraines correlate with glacio-fluvial deposits that were later dated MIS4 by Gribenski et al. (2021).

Southwestern foreland
Sample ART 18-01 (Figs. 2E, 3D) is the only large boulder preserved on the IMC in the East Lyonnais and Southwestern foreland (Fig. 3). It is also the largest (252 m^3) and tallest (~3.5 m) sampled boulder in the study (Fig. 2; Table 2). It yields an exposure age of 20.71 ± 0.90 ka. It is however situated on the internal slope of the moraine, rendering it vulnerable to incomplete exposure by partial burial or gravitational processes. Because of a lack of robustness due to the small amount of data, this age should be considered, with caution, as a minimum age of a glacier advance in the Southwestern foreland during the LGM.

The glacio-fluvial deposits dated as pre-LGM (Gribenski et al., 2021) in this area are correlated with IMC. The exposure age of ART 18-01 suggests that this glacial morphology is more complex and includes a stack of several glacier advances, the latest being LGM.

Crémieu plateau
In this sector (Fig. 3), the three samples have the same lithology (i.e., polygenic conglomerate, Table 2), therefore they come from the same polygenic conglomerate source located in the internal Alps and probably from the same rockfall on the glacier surface. According to Coutterand et al. (2009) and Coutterand (2010), this source corresponds to the "Flysch de Tarentaise." The oldest exposure age of the Crémieu plateau sector is HIL 20-01 at 497.48 ± 19.57 ka. This age is older than the oldest exposure age recorded from any sample obtained from the Alpine glaciations at 144.0 ± 5.3 ka (Graf et al., 2015). The ^{10}Be concentration measured for HIL 20-01 (~2330 × 10^3 atoms/g; Table 3) is of the same magnitude as a ^{10}Be concentration found on rock wall scars in the Mont Blanc Massif at an elevation >3400 m asl (Gallach et al., 2018). We hence interpret that the ^{10}Be concentration of HIL 20-01 is inherited from a prior exposure to cosmic rays on the original outcrop. Assuming that HIL 20-01 has followed a similar last exposure history as TRE 18-01, we can estimate the inherited ^{10}Be concentration (i.e., prior to last deposition and exposure event on the Crémieu plateau). This can be converted into an apparent exposure age of ca. 60 ka, when considering the highest altitude of the presumed rock source (~2900 m asl).

TRB 18-01 and TRE 18-01 boulders protrude 3.5 m and 3.0 m, respectively, from the ground (Table 2), and lie on a low elevated morainic landform (Fig. 4E), limiting incomplete exposure by burial or gravitational processes. These two samples yield similar exposure ages, and the older exposure age is TRE 18-01 at 18.81 ± 0.93 ka. This exposure age does not overlap within uncertainty with the other LGM exposure ages of the other sectors. It is therefore significantly younger and suggests a readvance or stabilization of the glaciers during the Late LGM.

Rhône Valley
The oldest exposure age of the Rhône Valley sector (Fig. 3) is YEN 19-01 at 21.80 ± 0.85 ka, corresponding to the LGM period. The YEN 19-01 sample is located on a bedrock ridge at 350 m asl, similar to the elevation of the Crémieu plateau boulders. Considering YEN 19-01 internal position and low elevation, the apparent exposure age is too old in comparison with the other samples giving LGM exposure ages located at higher elevation and/or farther in the foreland. Therefore, its overestimated age is probably explained by inheritance.

Excluding the YEN 19-01 sample, the oldest boulder on the Rhône Valley is CUL 19-01 at 16.50 ± 1.08 ka. This erratic boulder is the tallest (2.0 m high; Fig. 2; Table 2) sampled in the Rhône Valley sector. Despite the absence of significant geomorphological evidence allowing us to reconstitute the glacial front associated with CUL 19-01, the inner position and very low elevation (300 m asl) of this sample indicate that the lobe Lyonnais glacier remained in the foreland at least until 16.50 ± 1.08 ka during the late glacial period. This interpretation is supported by the ^{14}C ages (Fig. 1; Table 1) of human settlement in the same area (Romains cave 18.33–16.49 cal ka BP) and the Cerin Lake sediments (18.35–14.79 cal ka BP).

Reconstruction of extent and timing of the western French Alps glacier

Previous studies on glacial landforms in the French Alps foreland were based only on a relative chronology approach (Mandier, 1984; Roattino et al., 2021). Well-developed glacio-fluvial sediments that were dated by optically stimulated luminescence (OSL) techniques (Gribenski et al., 2021) provided MIS 4 and late MIS 3 ages. Glacio-fluvial deposit associated with the western morainic domain (Fig. 1) belong to the MIS 4. These moraines have never been directly dated because of the lack of boulders. In the same area, Vilain et al. (1988) studied the paleosol above the same till, providing consistent pre-LGM ^{14}C dates (Fig. 1; Table 1). These results evince important pre-LGM glacier extent during the last glacial period (Figs. 5, 6).

According to our results, dated moraines are at ca. 24–21 ka in Southern Jura, at ca. 23 ka in Terres Froides, and at ca. 21 ka in
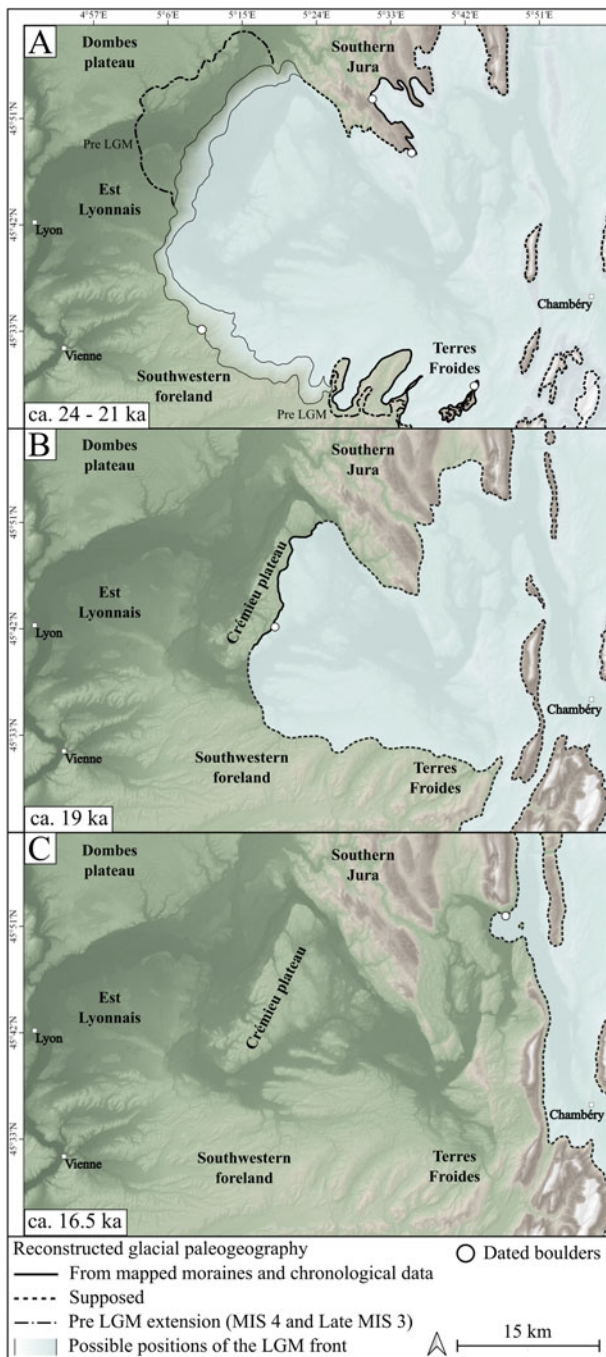
Figure 6. Reconstructed paleogeography of the Lyonnais ice lobe during the LGM. (**A**) Reconstruction between ca. 24–21 ka, solid lines are a glacial front based on the sets of moraines recognized and considered synchronous according to morphostratigraphical, pedological, and geological interpretations in previous studies and dated by our exposure ages. The gradient area delimited by thin solid lines represents the width of the intermediate morainic complex in the Southwestern foreland and Est Lyonnais where the position of the LGM front is not known precisely. Dotted lines represent supposed glacial fronts.

representative of a major glacier advance in the region during the LGM. This glacial stage should therefore be associated with main morphological features at the Lyonnais ice lobe scale. This is the case of the moraines from which the sampled glacial boulders come. In the foreland, the intermediate morainic domain is a continuous geomorphic feature running over a length of several tens of kilometers from Terres Froides to the Southwestern foreland and Est Lyonnais (Fig. 1). In Southern Jura, the outermost frontal moraines of Ordonnaz and Innimond are the locally best-preserved geomorphic expression of a glacier advance (Fig. 4). The LGM exposure ages therefore coincide with the major glacier advance features, both in the foreland and in the surrounding relief. The spatio-temporal correlation among these morainic domains appears to be the most plausible hypothesis.

These results do not allow a direct correlation between these morainic landforms and the glacio-fluvial deposits dated using OSL in the Southwestern area. However, they imply that, at least in this area, the two glacier extents (LGM and pre-LGM) are superimposed and confounded in morphology. Several hypothesis may then be considered to explain why LGM ages were not recorded in the OSL based dating: (1) the LGM ice front was not thick enough to overcome the topographic step allowing glacio-fluvial terrace aggradation observed beyond the intermediate morainic domain on Southwestern foreland; (2) considering that the ice front was thick enough, because OSL sampling targets were limited to sand lenses embedded in the glacio-fluvial sequences, a time delay between the levels sampled and the upper terrace surfaces could be possible; and (3) potential partial bleaching, common in glacial environments, would result in overestimated OSL ages. However, the resolution (single grain) at which the measurements were undertaken, as well as the use and concordance of multiple signals (quartz and feldspar) with varying bleaching properties, suggest reliability of the OSL ages.

On Crémieu plateau, dated moraines at ca. 19 ka are significantly younger than the dated moraines on Southern Jura, Terres Froides, and the Southwestern foreland. They are included in a more internal series of frontal moraines located on the Crémieu plateau and associated with a glacier readvance or stabilization phase (Enay, 1981; Steiner, 2020). This Late LGM age can be extended to the whole eastern morainic domain.

In the Rhône Valley sector, exposure ages indicate retreat of the glacier from the foreland at ca. 16.5 ka. The age of deglaciation of the western French Alps foreland is supported by radiocarbon data in the study area associated with post-glacial lacustrine, fluvial, and karst deposits (Fig. 1; Table 1).

Deglaciation of the western French Alps foreland between ca 19 ka and ca. 16.5 ka is consistent with the initiation of ice thinning in the western French Alps accumulation zones, more precisely in the Mont Blanc area at ca. 18.5 ka (Wirsig et al., 2016; Lehmann et al., 2020).

Our results are also in agreement with previous dating of the glaciers position at the entrance of the Romanche and Arc valleys at 17.5 ka and 15 ka, respectively (Schwartz et al., 2017; Prud'homme et al., 2020), and between 17.5–16 ka in the Arve valley (Coutterand and Nicoud, 2005; Perret, 2014).

Lyonnais ice lobe dynamics in the Alpine context

Our results can be used to establish a paleogeographic comparison between the Late Pleistocene advances of the Lyonnais ice lobe and the other Alpine foreland glaciers.

the Southwestern foreland. These exposure ages are considered as minimum ages. Theoretically, they could be much younger than the real glacier advance age. In this case, they would belong to pre-LGM glacier advances, and the LGM glacier may have not reached the front of the IMC.

However, the absence of older boulders belonging to the last glacial period in our dataset strongly suggests that these ages are

Pre-LGM glacier advances during MIS 4 have been documented in the Swiss Alps from OSL-dated fluvial and glacio-fluvial deposits (Preusser and Degering, 2007; Gaar and Preusser, 2019). The Italian foreland glaciers also show an interesting geometric relationship between the LGM moraines and earlier morainic landforms. An apparently smaller LGM advance than the pre-LGM extent also has been suggested for the Ivrea glacier lobe and Rivoli-Avigliana lobe, which share the Mont Blanc/Tarentaise and Maurienne accumulation zones with the Lyonnais ice lobe (Gianotti et al., 2008; Coutterand, 2010; Ivy-Ochs et al., 2018). Similar to the western morainic domain of the Lyonnais ice lobe, the pre-LGM dates of the Rivoli-Avigliana glacier moraines during the last glacial period are more external than the LGM moraines (Ivy-Ochs et al., 2018). Conversely, the other ice lobes in Italy and Switzerland reached their maximum extents during the LGM in the Alpine foreland (Wirsig et al., 2016; Monegato et al., 2017; Braakhekke et al., 2020).

LGM moraines in the western French Alps foreland dated between ca. 24–21 ka (Figs. 5, 6A) are consistent with the available chronology of the LGM foreland glaciers across the entire Alps. This result indicates synchronous LGM glacier extent of the western French Alps glacier with respect to the other alpine glacier systems.

The glacier readvance or stabilization phase of the Late LGM highlighted by the Crémieu plateau exposure age (ca. 19 ka) (Figs. 5, 6B) is also documented in the Italian foreland for the Rivoli-Avigliana glacier at 19.6 ± 0.9 ka (Ivy-Ochs et al., 2018), for the Ivrea glacier at 20.1 ± 3 (Gianotti et al., 2015), and for the Orta glacier at 19 ± 1 ka (Braakhekke et al., 2020). The innermost ice margin of the Verbano foreland glacier (dated at 19.7 ± 1.1 ka) has been correlated to a short-lived glacier readvance (Kamleitner et al., 2022). A Late LGM advance has been shown to have occurred between 22–17.5 ka on the Garda ice lobe (Monegato et al., 2017). In Switzerland, recessional moraines of the Reuss glacier have been dated at 18.6 ± 0.9 ka (Reber et al., 2014). These results show that the glacial landforms of the eastern morainic domain represent the effect of a major climatic stage, at least at the scale of the western Alps.

Western French Alps foreland deglaciation between ca. 19 ka and 16.5 ka (Figs. 5, 6C) is consistent with the initiation of ice thinning in the Alps accumulation zones between 18.5–14 ka (Dielforder and Hetzel, 2014; Hippe et al., 2014; Scapozza et al., 2014; Wirsig et al., 2016; Lehmann et al., 2020). Parallel to this ice surface lowering in the alpine accumulation zones, deglaciation of the Po plain foreland occurs between 18–17 ka (Gianotti et al., 2008; Lauterbach et al., 2012; Ravazzi et al., 2012, 2014; Gianotti et al., 2015; Serra et al., 2022). In the north-eastern part of the Alps, the withdrawal seems to be slightly older (20–18 ka; Lister, 1988; van Husen, 1997; Reitner, 2007; Schmidt et al., 2012; Fontana et al., 2014). Finally, our results will improve the modeling of alpine glacier dynamics during the last glacial cycle. Contrary to the results of previous models that lack dates, in our study area (Seguinot et al., 2018) our results show that the Lyonnais ice lobe returned to the piedmont during the LGM.

CONCLUSIONS

[10]Be surface-exposure dating of nine glacial boulders and 12 erratic boulders allowed us to investigate the glacial paleogeography of the western French Alps foreland during the global LGM. Our results provide the first evidence of the Lyonnais ice lobe extension in the piedmont area during the LGM. More precisely,

our data suggest that the intermediate morainic domain corresponds to a glacier advance between ca. 24–21 ka. Paleogeography highlighted by our dating and geomorphological mapping implies that the Lyonnais ice lobe extended over the foreland during the LGM, reaching pre-LGM glacier extent in the Southwestern foreland and Southern Jura areas. This paleoglacial extension of the Lyonnais ice lobe during the LGM is similar to that of the Ivrea and Rivoli-Avigliana glaciers (Italian Alps), which share similar accumulation areas. At ca. 19 ka, the eastern morainic domain was deposited by a readvance or stabilization phase. This phase is synchronous with the western Italian and Switzerland forelands ice lobes. According to our exposure ages and radiocarbon dates, after this phase, the Lyonnais ice lobe started a withdrawal phase and left the western French Alps foreland at ca.16.5 ka, which is in agreement with the timing of deglaciation of the western Italian foreland ice lobes. This synchronicity of glacial phases, at least at the scale of the Western Alps, suggests climatic forcing in glacier dynamics.

REFERENCES

Akçar, N., Ivy-Ochs, S., Kubik, P.W., Schlüchter, C., 2011. Post-depositional impacts on 'Findlinge' (erratic boulders) and their implications for surface-exposure dating. *Swiss Journal of Geosciences* **104**, 445–453.

Applegate, P., Lowell, T., Alley, R., 2007. Comment on "Absence of cooling in New Zealand and the adjacent ocean during the Younger Dryas chronozone." *Science* **320**, 746.

Arnold, M., Merchel, S., Bourlès, D.L., Braucher, R., Benedetti, L., Finkel, R.C., Aumaître, G., Gottdang, G., Klein, M., 2010. The French accelerator mass spectrometry facility ASTER: improved performance and developments. *Nuclear Instruments and Methods in Physics Research* **268**, 1954–1959.

Barrows, T., Lehman, S., Fifield, L., De Deckker, P., 2007. Absence of cooling in New Zealand and the adjacent ocean during the Younger Dryas chronozone. *Science* **318**, 86–89.

Becker, P., Seguinot, J., Jouvet, G., Funk, M., 2016. Last Glacial Maximum precipitation pattern in the Alps inferred from glacier modelling. *Geographica Helvetica* **71**, 173–187.

Bintz, P., Evin, J., 2002. Événements bio-climatiques et peuplements du Tardiglaciaire au début de l'Holocène dans les Alpes du nord Françaises. *Quaternaire* **13**, 279–287.

Bond, G., Broecker, W., Johnsen, S., McManus, J., Labeyrie, L., Jouzel, J., Bonani, G., 1993. Correlations between climate records from North Atlantic sediments and Greenland ice. *Nature* **365**, 143–147.

Bossuet, G., Ruffaldi, P., Magny, M., 1996. Dynamique et approche quantitative des remplissages fini- et postwürmiens du bassin lacustre de Cerin (Jura, France). *Bulletin de la Société Géologique de France* **167**, 483–494.

Braakhekke, J., Ivy-Ochs, S., Monegato, G., Gianotti, F., Martin, S., Casale, S., Christl, M., 2020. Timing and flow pattern of the Orta Glacier (European Alps) during the Last Glacial Maximum. *Boreas* **49**, 315–332.

Braucher, R., Guillou, V., Bourlès, D.L., Arnold, M., Aumaître, G., Keddadouche, K., Nottoli, E., 2015. Preparation of ASTER in-house ^{10}Be/^{9}Be standard solutions. *Nuclear Instruments and Methods in Physics Research B* **361**, 335–340.

Briner, J.P., Kaufman, D.S., Manley, W.F., Finkel, R.C., Caffee, M.W., 2005. Cosmogenic exposure dating of late Pleistocene moraine stabilization in Alaska. *Geological Society of America Bulletin* **117**, 1108–1120.

Brown, E., Molnar, P., Bourlès, D., 2005. Comment on "Slip-rate measurements on the Karakorum Fault may imply secular variations in Fault motion." *Science* **309**, 1326.

Brown, E.T., Edmond, J.M., Raisbeck, G.M., Yiou, F., Kurz, M.D., Brook, E.J., 1991. Examination of surface exposure ages of Antarctic moraines using in situ produced ^{10}Be and ^{26}Al. *Geochimica et Cosmochimica Acta* **55**, 2269–2283.

Buoncristiani, J.-F., Campy, M., 2011. Quaternary glaciations in the French Alps and Jura. In: Ehlers, J., Gibbard, P.L., Hughes, P.D. (Eds.), *Developments in Quaternary Sciences* 15, Elsevier, Amsterdam, pp. 117–126.

Chevalier, M.-L., Ryerson, F.J., Tapponnier, P., Finkel, R.C., Van Der Woerd, J., Haibing, L., Qing, L., 2005. Slip-rate measurements on the Karakorum Fault may imply secular variations in Fault motion. *Science* **307**, 411–414.

Clark, P.U., Dyke, A.S., Shakun, J.D., Carlson, A.E., Clark, J., Wohlfarth, B., Mitrovica, J.X., Hostetler, S.W., McCabe, A.M., 2009. The Last Glacial Maximum. *Science* **325**, 710–714.

Claude, A., Ivy-Ochs, S., Kober, F., Antognini, M., Salcher, B., Kubik, P.W., 2014. The Chironico landslide (Valle Leventina, southern Swiss Alps): age and evolution. *Swiss Journal of Geosciences* **107**, 273–291.

Cossart, E., Braucher, R., Fort, M., Bourlès, D.L., Carcaillet, J., 2008. Slope instability in relation to glacial debuttressing in alpine areas (upper Durance catchment, southeastern France): evidence from field data and ^{10}Be cosmic ray exposure ages. *Geomorphology* **95**, 3–26.

Cossart, E., Fort, M., Bourlès, D., Braucher, R., Perrier, R., Siame, L., 2012. Deglaciation pattern during the lateglacial/Holocene transition in the southern French Alps. Chronological data and geographical reconstruction from the Clarée Valley (upper Durance catchment, southeastern France). *Palaeogeography, Palaeoclimatology, Palaeoecology* **315–316**, 109–123.

Coutterand, S., 2010. *Étude Géomophologiques des Flux Glaciaires dans les Alpes Nord-occidentales au Pléistocène Récent. Du Maximum de la Dernière Glaciation aux Premières Étapes de la Déglaciation*. Ph.D. dissertation, Université Savoie Mont Blanc, Chambéry, France, 468 pp.

Coutterand, S., Nicoud, G., 2005. Les stades de retrait du glacier de l'Arve entre le verrou de Cluses et l'ombilic de Chamonix au cours du Tardiglaciaire (Vallée de l'Arve, Haute-Savoie). *Quaternaire* **2**, 85–94.

Coutterand, S., Schoeneich, P., Nicoud, G., 2009. Le lobe glaciaire Lyonnais au maximum würmien glacier du Rhône ou/et glaciers savoyards?. *Collection EDYTEM, Cahiers de Géographie* **8**, 9–20.

David, L., Enay, R., Mangold, C., 1978. *Notice Explicative et Carte Géologique France (1/50 000), feuille Montuel (699)*. Orléans, Bureau de Recherches Géologiques et Minières (BRGM).

Dielforder, A., Hetzel, R., 2014. The deglaciation history of the Simplon region (southern Swiss Alps) constrained by ^{10}Be exposure dating of ice-molded bedrock surfaces. *Quaternary Science Reviews* **84**, 26–38.

Doyen, E., Vannière, B., Rius, D., Bégeot, C., Millet, L., 2015. Climate and biomass control on fire activity during the late-glacial/early-Holocene transition in temperate ecosystems of the upper Rhone valley (France). *Quaternary Research* **83**, 94-104.

Ehlers, J., Gibbard, P. L., Hughes, P. D., 2011. *Quaternary Glaciations—Extent and Chronology. A Closer Look*. Elsevier, Amsterdam, 1108 pp.

Elmi, S., Enay, R., Mangold, C., Mongereau, N., 1986. *Notice Explicative et Carte Géologique France (1/50 000), feuille Bourgoin-Jaillieu (723)*. Orléans, Bureau de Recherches Géologiques et Minières (BRGM).

Emiliani, C., 1955. Pleistocene temperatures. *Journal of Geology* **63**, 538–578.

Enay, R., 1981. Les formations glaciaires et les stades de retrait du glacier würmien dans l'Ile Crémieu. *Bulletin de la Société Linnéenne de Lyon* **50**, 5–27.

Evin, J., Marechal, J., Marien, G., 1985. Lyon natural radiocarbon measurements X. *Radiocarbon* **27**, 386–454.

Federici, P.R., Granger, D.E., Ribolini, A., Spagnolo, M., Pappalardo, M., Cyr, A.J., 2012. Last Glacial Maximum and the Gschnitz stadial in the Maritime Alps according to ^{10}Be cosmogenic dating. *Boreas* **41**, 277–291.

Federici, P. R., Ribolini, A., Spagnolo, M., 2016. Glacial history of the Maritime Alps from the Last Glacial Maximum to the Little Ice Age. In: Hughes, P.D., Woodward, J.C. (Eds.), Quaternary Glaciation in the Mediterranean Mountains: *Geological Society London Special Publication* 433, 137–159.

Fontana, A., Monegato, G., Zavagno, E., Devoto, S., Burla, I., Cucchi, F., 2014. Evolution of an Alpine fluvioglacial system at the LGM decay. The Cormor megafan (NE Italy). *Geomorphology* **204**, 136–153.

Gaar, D., Preusser, F., 2019. New chronological constraints on the timing of Late Pleistocene glacier advances in Northern Switzerland. *E & G Quaternary Science Journal* **68**, 53–73.

Gallach, X., Egli, M., Brandova, D., Schaepman, M., Christl, M., Gruber, S., Deline, P., Carcaillet, J., Pallandre, F., 2018. Timing of rockfalls in the Mont Blanc massif (Western Alps): evidence from surface exposure dating with cosmogenic ^{10}Be. *Landslides* **15**, 1991–2000.

Gianotti, F., Forno, M.G., Ivy-Ochs, S., Kubik, P.W., 2008. New chronological and stratigraphical data on the Ivrea amphitheatre (Piedmont, NW Italy). *Quaternary International* **190**, 123–135.

Gianotti, F., Forno, M.G., Ivy-Ochs, S., Monegato, G., Pini, R., Ravazzi, C., 2015. Stratigraphy of the Ivrea morainic amphiteatre (NW Italy): an updated synthesis. *Alpine and Mediterranean Quaternary* **28**, 29–58.

Gigout, M., Enay, R., Pierre, G., Rampnoux, J.-P., 1976. *Notice Explicative et Carte Géologique France (1/50 000), feuille La Tour du Pin (724)*. Orléans, Bureau de Recherches Géologiques et Minières (BRGM).

Graf, A., Akçar, N., Ivy-Ochs, S., Strasky, S., Kubik, P. W., Christl, M., Burkhard, M., Wieler, R., Schlûchter, C., 2015. Multiple advances of Alpine glaciers into the Jura Mountains in the Northwestern Switzerland. *Swiss Journal of Geosciences* **108**, 225–238.

Gribenski, N., Valla, P.G., Preusser, F., Roattino, T., Crouzet, C., Buoncristiani, J.-F., 2021. Out-of-phase Late Pleistocene glacier advances in the Western Alps reflect past changes in North Atlantic atmospheric circulation. *Geology* **49**, 1096–1101.

Grootes, P.M., Stulver, M., White, J.W.C., Johnsen, S., Jouzel, J., 1993. Comparison of oxygen isotope records from the GISP2 and GRIP Greenland ice cores. *Nature* **366**, 552–554.

Heyman, J., Stroeven, A.P., Harbor, J.M., Caffee, M.W., 2011. Too young or too old: evaluating cosmogenic exposure dating based on an analysis of compiled boulder exposure ages. *Earth and Planetary Science Letters* **302**, 71–80.

Heyman, J., Applegate, P.J., Blomdin, R., Gribenski, N., Harbor, J.M., Stroeven, A.P., 2016. Boulder height—exposure age relationships from a global glacial ^{10}Be compilation. *Quaternary Geochronology* **34**, 1–11.

Hippe, K., Ivy-Ochs, S., Kober, F., Zasadni, J., Wieler, R., Wacker, L., Kubik, P.W., Schlüchter, C., 2014. Chronology of Lateglacial ice flow reorganization and deglaciation in the Gotthard Pass area, Central Swiss Alps, based on cosmogenic ^{10}Be and in situ ^{14}C. *Quaternary Geochronology* **19**, 14–26.

Ivy-Ochs, S., 2015. Glacier variations in the European Alps at the end of the last glaciation. *Cuadernos de Investigacion Geografica* **41**, 295–315.

Ivy-Ochs, S., Schäfer, J., Kubik, P.W., Synal, H.-A., Schlüchter, C., 2004. Timing of deglaciation on the northern Alpine foreland (Switzerland). *Eclogea Geologicae Helvetiae* **97**, 47–55.

Ivy-Ochs, S., Lucchesi, S., Baggio, P., Fioraso, G., Gianotti, F., Monegato, G., Graf, A.A., Akçar, N., Christl, M., Carraro, F., 2018. New geomorphological and chronological constraints for glacial deposits in the Rivoli-Avigliana end-moraine system and the lower Susa Valley (Western Alps, NW Italy). *Journal of Quaternary Science* **33**, 550–562.

Jorda, M., 1988. Modalités paléoclimatiques et chronologiques de la déglaciation würmienne dans les Alpes Françaises du Sud (Bassin durancien et Alpes de Haute Provence). *Bulletin de l'Association Française pour l'Étude du Quaternaire* **25**, 111–122.

Kamleitner, S., Ivy-Ochs, S., Monegato, G., Gianotti, F., Akçar, N., Vockenhuber, C., Christl, M., Synal, H.-A., 2022. The Ticino-Toce glacier system (Swiss-Italian Alps) in the framework of the Alpine Last Glacial Maximum. *Quaternary Science Reviews* **279**, 107400. https://doi.org/10.1016/j.quascirev.2022.107400.

Kerrien, Y., Monjuvent, G., 1990. *Notice explicative de la Carte Géologique de la France (1/50 000), feuille Belley (700)*. Orléans, Bureau de Recherches Géologiques et Minières (BRGM).

Lambeck, K., Rouby, H., Purcell, A., Sun, Y., Sambridge, M., 2014. Sea level and global ice volumes from the Last Glacial Maximum to the Holocene. *PNAS* 111, 15296–15303.

Lauterbach, S., Chapron, E., Brauer, A., Hüls, M., Gilli, A., Arnaud, F., Piccin, A., *et al.*, 2012. A sedimentary record of Holocene surface runoff events and earthquake activity from Lake Iseo (Southern Alps, Italy). *The Holocene* 22, 749–760.

Le Roy, M., Deline, P., Carcaillet, J., Schimmelpfenning, I., Ermini, M., ASTER Team., 2017. [10]Be exposure dating of the timing of neoglacial glacier advances in the Ecrins-Pelvoux massif, southern French Alps. *Quaternary Science Reviews* 178, 118–138.

Lehmann, B., Herman, F., Valla, P.G., King, G.E., Biswas, R.H., Ivy-Ochs, S., Steinemann, O., Christl, M., 2020. Postglacial erosion of bedrock surfaces and deglaciation timing. New insights from the Mont Blanc massif (western Alps). *Geology* 48, 139–144.

Lifton, N., 2016. Implications of two Holocene time-dependent geomagnetic models for cosmogenic nuclide production rate scaling. *Earth and Planetary Science Letters* 433, 257–268.

Lifton, N., Sato, T., Dunai, T.J., 2014. Scaling in situ cosmogenic nuclide production rates using analytical approximations to atmospheric cosmic-ray fluxes. *Earth and Planetary Science Letters* 386, 149–160.

Lisiecki, L.E., Raymo, M.E., 2005. A Pliocene–Pleistocene stack of 57 globally distributed benthic $\partial^{18}O$ records. *Paleoceanography* 20, PA1003. https://doi.org/10.1029/2004PA001071.

Lister, G.S., 1988. A 15,000-year isotopic record from Lake Zürich of deglaciation and climatic change in Switzerland. *Quaternary Research* 29, 129–141.

Loebell, A., 1980. Les quinze derniers milénaires en Jura méridional, etudes sédimentologiques de trois sites. *Bulletin de l'Association Française pour l'Étude du Quaternaire* 3, 143–153.

Mandier, P., 1984. *Le Relief de la Moyenne Vallée du Rhône au Tertiaire et au Quaternaire. Essai de Synthèse Paléogéographie.* Ph.D. dissertation, Lyon, Université Lumière Lyon 2, 654 pp.

Mandier, P., 1988. Les problèmes chronologiques posés par les phases de la récession würmienne dans la moyenne vallée du Rhône. *Bulletin de l'Association Française pour l'Etude du Quaternaire* 25, 123–128.

Mandier, P., Piegay, H., 1991. Elements nouveaux sur les phases de recession du glacier rhodanien dans la region des Terres Froides septentrionales autour de Morestel. *Bulletin du Laboratoire Rhodanien de Géomorphologie* 28, 23–53.

Mandier, P., Evin, J., Argant, J., Petiot, R., 2003. Chronostratigraphie des accumulation wurmiennes dans la moyenne vallée du Rhône. L'apport des dates radiocarbone. *Quaternaire* 14, 113–127.

Martin, L., Blard, P.-H., Balco, G., Lavé, J., Delunel, R., Lifton, N., Laurent, V., 2017. The CREp program and the ICE-D production rate calibration database: a fully parameterizable and updated online tool to compute cosmic-ray exposure ages. *Quaternary Geochronology* 38, 25–49.

Merchel, S., Herpers, U., 1999. An update on radiochemical separation techniques for the determination of long-lived radionuclides via accelerator mass spectrometry. *Radiochimica Acta* 84, 215–219.

Mey, J., Scherler, D., Wickert, A.D., Egholm, D.L., Tesauro, M., Schildgen, T.F., Strecker, M.R., 2016. Glacial isostatic uplift of the European Alps. *Nature Communication* 7, 13382. https://doi.org/10.1038/ncomms13382.

Monegato, G., Ravazzi, C., Donegana, M., Pini, R., Calderoni, G., Wick, L., 2007. Evidence of a two-fold glacial advance during the last glacial maximum in the Tagliamento end moraine system (eastern Alps). *Quaternary Research* 68, 284–302.

Monegato, G., Scardia, G., Hajdas, I., Rizzini, F., Piccin, A., 2017. The Alpine LGM in the boreal ice-sheet game. *Scientific Reports* 7, 2078. https://doi.org/10.1038/s41598-017-02148-7.

Monjuvent, G., 1988. La déglaciation rhodanienne entre les moraines internes et le val du Bourget. *Géologie Alpine* 64, 62–104.

Monjuvent, G., Nicoud, G., 1988. Modalités et chronologie de la déglaciation würmienne dans l'arc alpin occidental et les massifs français : synthèse et réflexions. *Bulletin de l'Association Française pour l'Etude du Quaternaire* 25, 147–156.

Monjuvent, G., Combier, J., Michel, R., 1980. *Notice explicative de la Carte Géologique de la France (1/50 000), feuille La Côte-St-André (747).* Orléans, Bureau de Recherches Géologiques et Minières (BRGM).

Penck, A., Brückner, E., 1901–1909. *Die Alpen im Eiszeitalter.* Tauchnitz, Leipzig, 1199 pp.

Perret, A., 2014. *Géopatrimoine des trois Chablais: Identification et Valorisation des Témoins Glaciaires.* Ph.D. thesis, Université Savoie Mont Blanc, Chambéry, France, 266 pp.

Petit, J.R., Jouzel, J., Raynaud, D., Barkov, N.I., Barnola, J.-M., Basile, I., Bender, M., 1999. Climate and atmospheric history of the past 420,000 years from the Vostok ice core, Antarctica. *Nature* 399, 429–436.

Preusser, F., Degering, D., 2007. Luminescence dating of the Niederweningen mammoth site, Switzerland. *Quaternary International* 164–165, 106–112.

Protin, M., 2019. Preliminary work on reduced glacier extents and subglacial erosion rates in the Mont-Blanc massif. In: Protin M., *Études des Fluctuations Glaciaires dans le Massif du Mont-Blanc depuis la fin du Dryas Récent à Partir des Nucléides Cosmogéniques in situ.* Ph.D. thesis, Université Aix Marseille, Marseille, France, 204 pp.

Protin, M., Schimmelpfenning, I., Mugnier, J.-L., Ravanel, L., Le Roy, M., Deline, P., Favier, V., Buoncristiani, J.-F., ASTER Team., 2019. Climatic reconstruction for the Younger Dryas/Early Holocene transition and the Little Ice Age based on paleo-extents of Argentiere glacier (French Alps). *Quaternary Science Reviews* 221, 105863. https://doi.org/10.1016/j.quascirev.2019.105863.

Prud'homme, C., Vassallo, R., Crouzet, C., Carcaillet, J., Mugnier, J.-L., Cortés-Aranda, J., 2020. Paired [10]Be sampling of polished bedrock and erratic boulders to improve dating of glacial landforms. an example from the Western Alps. *Earth Surface Processes and Landforms* 45, 1168–1180.

Putkonen, J., Swanson, T., 2003. Accuracy of cosmogenic ages for moraines. *Science Direct* 59, 255–261.

Ravazzi, C., Badino, F., Marsetti, D., Patera, G., Reimer, P.J., 2012. Glacial to paraglacial history and forest recovery in the Oglio glacier system (Italian Alps) between 26 and 15 ka cal BP. *Quaternary Science Reviews* 58, 146–161.

Ravazzi, C., Pini, R., Badino, F., De Amicis, M., Londeix, L., Reimer, P.J., 2014. The latest LGM culmination of the Garda Glacier (Italian Alps) and the onset of glacial termination. Age of glacial collapse and vegetation chronosequence. *Quaternary Science Reviews* 105, 26–47.

Reber, R., Akçar, N., Ivy-Ochs, S., Tikhomirov, D., Burkhalter, R., Zahno, C., Lüthold, A., Kubik, P.W., Vockenhuber, C., Christian, S., 2014. Timing of retreat of the Reuss Glacier (Switzerland) at the end of the Last Glacial Maximum. *Swiss Journal of Geosciences* 107, 293–307.

Reimer, P.J., Austin, W.E.N., Bard, E., Bayliss, A., Blackwell, P.G., Ramsey, B.C., Butzin, M., *et al.*, 2020. The IntCal20 Northern Hemisphere Radiocarbon Age Calibration Curve (0–55 cal kBP). *Radiocarbon* 62, 725–757.

Reitner, J., 2007. Glacial dynamics at the beginning of Termination I in the Eastern Alps and their stratigraphic implications. *Quaternary International* 164–165, 64–84.

Roattino, T., Crouzet, C., Buoncristiani, J.-F., Tissoux, H., 2021. Geometry of glaciofluvial deposits and dynamics of the Lyonnais lobe ice front during last glacial period (France, Northern Alps). *Earth Sciences Bulletin* 192, 21. https://doi.org/10.1051/bsgf/2021012.

Scapozza, C., Castelletti, C., Soma, L., Dall'Agnolo, S., Ambrosi, C., 2014. Timing of LGM and deglaciation in the Southern Swiss Alps. *Quaternary Geomorphology* 20, 307–322.

Schmidt, R., Weckström, K., Lauterbach, S., Tessadri, R., 2012. North Atlantic climate impact on early late-glacial climate oscillations in the southeastern Alps inferred from a multi-proxy lake sediment record. *Journal of Quaternary Science* 27, 40–50.

Schoeneich, P., 1998. Corrélation du dernier maximum glaciaire et de la déglaciation alpine avec l'enregistrement isotopique du Groenland. *Quaternaire* 9, 203–215.

Schwartz, S., Zerathe, S., Jongmans, D., Baillet, L., Carcaillet, J., Audin, L., Dumont, T., Bourlès, D., Braucher, R., Lebrouc, V., 2017. Cosmic ray exposure dating on the large landslide of Séchilienne (Western Alps). A synthesis to constrain the slope evolution. *Geomorphology* 278, 329–244.

Seguinot, J., Ivy-Ochs, S., Jouvet, G., Huss, M., Funk, M., Preusser, F., 2018. Modelling last glacial cycle ice dynamics in the Alps. *The Cryosphere* 12, 3265–3285.

Shackleton, N.J., 1987. Oxygen isotopes, ice volume and sea level. *Quaternary Science Reviews* 6, 183–190.

Serra, E., Valla, P.G., Gribenski, N., Carcaillet, J., Deline, P., 2022. Post-LGM glacial and geomorphic evolution of the Dora Baltea valley

(western Italian Alps). *Quaternary Science Reviews* **282**, 107446. https://doi.org/10.1016/j.quascirev.2022.107446.

Starnberger, R., Rodnight, H., Spötl, C., 2011. Chronology of the Last Glacial Maximum in the Salzach palaeoglacier area (Eastern Alps). *Journal of Quaternary Science* **26**, 502–510.

Steiner, S.G., 2020. *Etude Géomorphologique, Cartographique et Sédimentaire des dépôts Würmiens dans la région de Lyon, France.* Master 2 internship report, Université de Bourgogne, Dijon, France, 50 pp.

Steinfatt, E., 1975. *Géologie de la feuille Voiron au 1/50 000. Etudes sur le Miocène et le Quaternaire de l'avant Pays Alpin.* Ph.D. thesis, Université Scientifique et Médicale de Grenoble, Grenoble, France, 76 pp.

Tomkins, M.D., Dortch, J.M., Hughes, P.D., Huck, J.J., Pallàs, R., Rodés, Á., Allard, J., *et al.*, 2021. Moraine crest or slope: An analysis of the effects of boulder position on cosmogenic exposure age. *Earth and Planetary Science Letters* **570**, 117092. https://doi.org/10.1016/j.epsl.2021.117092.

Uppala, S.M., Kållberg, P.W., Simmons, A.J., Andrea, U., Da Costa Bechtold, V., Fiorino, M., Gibson, J.K., *et al.*, 2005. The ERA-40 re-analysis. *Quaternary Journal of the Royal Meteorological Society* **131**, 2961–3012.

van Husen, D., 1997. LGM and late-glacial fluctuations in the Eastern Alps. *Quaternary International* **38/39**, 109–118.

Vilain, R., Evin, J., Drevon, G., Marechal, J., 1988. Nouvelles observations géologiques et datations absolues dans le complexe morainique wurmien de Balan (Ain, France). *Bulletin des Naturalistes et Archéologues de l'Ain* **8**, 457–468.

Višnjević, V., Herman, F., Prasicek, G., 2020. Climatic patterns over the European Alps during the LGM derived from inversion of the paleo-ice extent. *Earth and Planetary Science Letters* **538**, 116185. https://doi.org/10.1016/j.epsl.2020.116185.

Wirsig, C., Zasadni, J., Christl, M., Akçar, N., Ivy-Ochs, S., 2016. Dating the onset of LGM ice surface lowering in the High Alps. *Quaternary Science Reviews* **143**, 37–50.